Nucleic Acids Research, 2025, **53**, gkaf149
https://doi.org/10.1093/nar/gkaf149
Molecular and Structural Biology

Structural basis of TnsC oligomerization and transposase recruitment in type I-B CRISPR-associated transposons

Giada Finocchio[1], Irma Querques[1,2], Christelle Chanez[1], Katarzyna J. Speichert[1], Martin Jinek[1,*]

[1]Department of Biochemistry, University of Zurich, 8057 Zurich, Switzerland
[2]Present address: Department of Structural and Computational Biology, Max Perutz Labs, University of Vienna, 1030 Vienna, Austria
[*]To whom correspondence should be addressed. Email: jinek@bioc.uzh.ch

Abstract

CRISPR-associated transposon (CAST) systems employ CRISPR–Cas systems as RNA-directed targeting modules for site-specific transposon DNA insertion. Among them, type I CASTs rely on the coordinated action of the guide RNA-bound Cascade complex and the transposon proteins TniQ, TnsC, and TnsAB. The interaction between the transposase TnsAB and the ATPase TnsC is crucial for transposition activity, yet the underlying molecular details have remained elusive. Here, we investigate the type I-B CAST system from *Peltigera membranacea cyanobiont*. Cryo-electron microscopic structures of TnsC and its complex with the C-terminal region of TnsAB reveal that TnsC forms a heptameric ring that recruits TnsAB by interacting with its C-terminal tail. *In vitro* binding assays indicate that TnsAB exclusively interacts with the TnsC heptamer without inducing its disassembly, in contrast to type V-K CAST systems. Mutational analysis of key structural features corroborates the significance of TnsC multimerization and TnsB interaction for transposon activity *in vivo*. Altogether, these findings offer detailed structural and functional insights into the molecular mechanism of type I-B CAST, with the aim of facilitating their development as genome engineering tools.

Graphical abstract

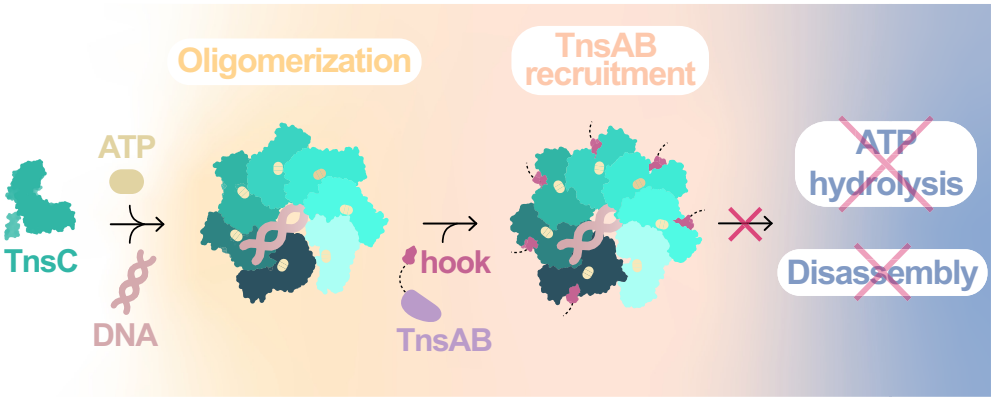

Introduction

Transposons are ubiquitous mobile genetic elements capable of mobilizing within and between host genomes by adopting various strategies [1, 2]. This process, termed transposition, is catalyzed by transposase enzymes encoded within the boundaries (ends) of the transposon DNA [3, 4]. The Tn7 element from *Escherichia coli* (*E. coli*) is one of the best-studied bacterial transposons to date [5–7]. It encodes two transposase subunits, TnsA and TnsB, along with the AAA + ATPase TnsC and target site selector proteins TnsE and TnsD [5, 6]. TnsA and TnsB together recognize the transposon left end (LE) and right end (RE) sequences to form a paired-end complex (PEC), cleaving the ends to generate their 5′ and 3′ termini, respectively. TnsB subsequently catalyzes the integration of the transposon DNA into a target site upon the formation of a target capture complex. Tn7 can insert into a specific host genomic locus through the TnsD-mediated pathway [8, 9] or integrate into conjugative plasmids using TnsE [10]. In both transposition modes, TnsC is thought to recognize the target selector protein [11, 12] and recruit the PEC to the target DNA [13].

CRISPR-associated transposons (CASTs) are Tn7-like elements that have co-opted a nuclease-deficient CRISPR–Cas system as their RNA-guided targeting module, functionally replacing the TnsE target selector protein [14–21]. Type V CASTs depend on a single catalytically inactive Cas12k

Received: September 23, 2024. **Revised:** February 11, 2025. **Editorial Decision:** February 12, 2025. **Accepted:** February 20, 2025

protein [16], while type I CASTs rely on a multi-subunit effector complex termed Cascade [22], which lacks the canonical helicase-nuclease Cas3 [17]. CASTs use CRISPR-array encoded RNA guides to mediate site-specific transposition [16, 17, 19]. The programmable DNA insertion specificity of CASTs has been exploited to develop these systems as molecular genetic engineering tools for the homology-independent insertion of large DNA payloads [23]. Type I CASTs are particularly promising due to their high fidelity cut-and-paste transposition mechanism, high efficiency, and intrinsic precision [17, 24, 25], while type V CASTs [16, 26] transpose by a copy-and-paste mechanism and exhibit considerable levels of guide RNA-independent transposition activity [26].

Structural and biochemical studies of the *Scytonema hofmanni* type V-K CAST (ShCAST) have shed light on the interactions underpinning the assembly of the transpososome holocomplex [27–33], revealing an unexpected role for the host ribosomal protein S15. Structural analyses of the *Vibrio cholerae* I-F (VchCAST) [34–36] and the *Peltigera membranacea cyanobiont 210A* I-B (PmcCAST) [37] systems have in turn revealed the mechanisms of RNA-guided target binding and TniQ-dependent TnsC assembly. In both type I systems, TnsC forms heptameric ring-like assemblies in an ATP-dependent manner [37, 38], whereas the ShCAST TnsC forms polymeric filaments whose disassembly is controlled by interactions with the single-subunit transposase TnsB. Despite these advances, we still lack detailed understanding of the molecular role of TnsC in transpososome assembly in type I CAST systems.

Here, we provide structural insights into the assembly of the type I-B TnsC from the PmcCAST system and its interaction with the transposase fusion protein TnsAB. Using cryogenic electron microscopy (cryo-EM), we show that PmcTnsC forms a heptameric ring in the presence of DNA and AMPPNP. Mutational analysis of key residues validates the importance of ring assembly, nucleotide binding, and hydrolysis for functional transposition *in vivo*. A cryo-EM structure of PmcTnsC in complex with a C-terminal region of TnsAB reveals that the transposase binds TnsC at the periphery of the ATPase site, without impacting nucleotide binding. We find that PmcTnsAB is unable to induce the disassembly of PmcTnsC oligomers *in vitro*. Collectively, these findings shed light on the function of TnsC in type I CAST systems and highlight their mechanistic differences with type V CASTs.

Materials and methods

DNA constructs

The primers used to construct plasmids are listed in Supplementary Table S2. The DNA sequence encoding *Peltigera membranacea cyanobiont 210A* (Pmc) TnsC was codon optimized for heterologous expression in *E. coli*, synthesized by GeneArt with flanking overhangs (Thermo Fisher Scientific) and amplified from the template using the primers TnsC_f and TnsC_r (Supplementary Table S2). Polymerase chain reaction (PCR) products were inserted into the 1S (Addgene #29659) or 1C (Addgene #29654) vectors using ligation-independent cloning (LIC) [39], resulting in constructs carrying an N-terminal hexahistidine-SUMO tag (His_6-SUMO) followed by a tobacco etch virus (TEV) cleavage site or an N-terminal hexahistidine-maltose binding protein tag (His_6-MBP) followed by a TEV cleavage site, respectively. The *tnsAB* gene was amplified by PCR with the primers TnsAB_f and TnsAB_r (Supplementary Table S2) using the vector pHelper (PmcCAST)_PmcPSP1 (Addgene #168151) as a template. The $tnsAB^{855\text{-}898}$ gene truncation was obtained by PCR with the primers TnsAB_CTD_f and TnsAB_r (Supplementary Table S2) using the same template. The PCR products were inserted into 1C vectors using LIC.

Point mutations in the TnsC and TnsAB protein sequences were introduced by Gibson assembly [40] using gBlock gene fragments (IDT). The pDonor (Addgene #168162), pHelper (Addgene #168151), and pHelper_Δspacer (Addgene #168154) plasmids used in droplet digital PCR (ddPCR) experiments were sourced from Addgene. To remove the *tRNA* gene from the pTarget vector, a pTarget_ΔtRNA vector was created by Gibson assembly between two fragments amplified from the template pTarget (PmcCAST) (Addgene #168163) using the primers pTarget_ΔtRNA_1_f with pTarget_ΔtRNA_1_r, and pTarget_ΔtRNA_2_f with pTarget_ΔtRNA_2_r (Supplementary Table S2). A positive control plasmid for ddPCR was generated by Gibson cloning between an insert amplified from pDonor (with primers Control+_1_f and Control+_1_r, Supplementary Table S2) and pTarget_ΔtRNA (linearized with primers Control+_2_f and Control+_2_r, Supplementary Table S2). The control plasmid simulated the product of a successful jump of the transposon DNA from pDonor to pTarget_ΔtRNA with a left end–right end (LE–RE) orientation. Plasmids were cloned and propagated in Mach1 cells (Thermo Fisher Scientific). Plasmids were purified using the GeneJET Plasmid Miniprep Kit (Thermo Fisher Scientific) and verified by Sanger sequencing (MicroSynth AG).

Protein expression and purification

For expression of wild-type (WT) PmcTnsC, His_6-SUMO-tagged or His_6-MBP-tagged PmcTnsC was expressed in BL21 Rosetta2 (DE3) cells (Novagen). Cell cultures were grown at 37°C shaking at 110 rpm until an OD_{600} of 0.6 was reached. Protein expression was induced with 0.2 mM isopropyl-β-D-1-thiogalactopyranoside (IPTG) and continued for 16 h at 18°C. Harvested cells from 3 l of culture were resuspended in 60 ml of lysis buffer (20 mM Tris–HCl, pH 7.5, 500 mM NaCl, 5 mM imidazole, 10% glycerol) supplemented with 1 μg/ml pepstatin, 200 μg/ml AEBSF, and 1 μg/ml DNAse. The resuspended cells solution was lysed by ultrasonication (Bandelin Sonopuls HD 3200 equipped with a VS 70 T probe, 1 s-on/2 s-off cycle, 30% amplitude, 15 min total). The lysate was cleared of cell debris by centrifugation at 40 000 *g* for 30 min at 4°C. The cleared sample was applied to two 5 ml Ni-NTA cartridges (Qiagen). The column was washed in three steps (40 ml each) with lysis buffer supplemented with 5, 25, and 50 mM imidazole, and bound proteins were eluted with 40 ml of the same buffer supplemented with 100 mM imidazole. Elution fractions were pooled and dialyzed overnight in 2 l of 20 mM Tris–HCl, pH 7.5, 200 mM NaCl, 10% glycerol, and 1 mM dithiothreitol (DTT) in the presence of His_6-tagged TEV protease. Dialyzed proteins were loaded in a 5 ml of HiTrap Heparin HP column (Cytiva) and eluted with a linear gradient of 20 mM Tris–HCl, pH 7.5, 1 M NaCl, 5% glycerol, and 1 mM DTT in 100 ml (target buffer concentration 80%). Elution fractions were pooled, concentrated using 30 000 molecular weight cut-off centrifugal filters (Merck Millipore) and further purified by size-exclusion chromatog-

raphy using a Superdex 200 Increase 10/300 GL column (Cytiva) in 20 mM Tris–HCl, pH 7.5, 500 mM NaCl, 1 mM DTT yielding pure, and monodisperse proteins. Purified TnsC was concentrated to 10–15 mg/ml using 30 000 molecular weight cut-off centrifugal filters (Merck Millipore) and flash-frozen in liquid nitrogen.

For expression of WT TnsAB, His_6-MBP tagged PmcTnsAB was expressed in *E. coli* BL21 Star (DE3) cells (Thermo Fisher Scientific). Cell cultures were grown at 37°C shaking at 110 rpm until an OD_{600} of 0.6 was reached. Protein expression was induced with 0.4 mM IPTG and continued for 16 h at 18°C. Harvested cells from 6 l of culture were resuspended in 120 ml of lysis buffer (20 mM Tris–HCl, pH 7.5, 500 mM NaCl, 5 mM imidazole, and 5% glycerol) supplemented with 1 μg/ml pepstatin, 200 μg/ml AEBSF, and 1 μg/ml DNAse. The resuspended cells solution was lysed by ultrasonication (Bandelin Sonopuls HD 3200, 1-s on, 2-s off cycle, 30% amplitude, 15 min in total, VS 70 T probe). The lysate was cleared of cell debris by centrifugation at 40 000 *g* for 35 min at 4°C. The cleared sample was applied to two 5 ml of Ni-NTA cartridges (Qiagen). The column was washed in two steps (40 ml each) with lysis buffer supplemented with 5 or 25 mM imidazole, and bound proteins were eluted in two steps (40 ml each) of the same buffer supplemented with 50 or 100 mM imidazole. Elution fractions were pooled and dialyzed overnight in 2 l of 20 mM Tris–HCl, pH 7.5, 200 mM NaCl, and 1 mM DTT in the presence of His_6-tagged TEV protease. Dialyzed proteins were loaded in a 5 ml of HiTrap Heparin HP column (Cytiva) and eluted with a linear gradient of 20 mM Tris–HCl, pH 7.5, 1 M NaCl, and 1 mM DTT in 180 ml (target buffer concentration 70%). Elution fractions were pooled, concentrated using 30 000 molecular weight cut-off centrifugal filters (Merck Millipore) and further purified by size-exclusion chromatography using a Superdex 200 Increase 10/300 GL column (Cytiva) in 20 mM Tris–HCl, pH 7.5, 500 mM NaCl, 1 mM DTT yielding pure, and monodisperse proteins. Purified TnsAB was concentrated to 10–15 mg/ml using 30 000 molecular weight cut-off centrifugal filters (Merck Millipore) and flash-frozen in liquid nitrogen. For the expression and purification of His_6-MBP-tagged TnsAB, the same procedure as for WT PmcTnsAB was followed, with the only difference being that the TEV-cleavage and heparin steps were omitted.

For the expression of His_6-MBP-tagged $TnsAB^{855\text{-}898}$ ($TnsAB^{CTD}$), a similar procedure as for WT PmcTnsAB was followed. Harvested cells from 3 l of culture were resuspended in 60 ml of lysis buffer (20 mM Tris–HCl, pH 7.5, 500 mM NaCl, and 5% glycerol) supplemented with 1 μg/ml pepstatin, 200 μg/ml AEBSF, and 1 μg/ml DNAse. The resuspended cells solution was lysed by ultrasonication (Bandelin Sonopuls HD 3200, 1-s on, 2-s off cycle, 30% amplitude, 15 min in total, and VS 70 T probe). The lysate was cleared of cell debris by centrifugation at 40 000 *g* for 30 min at 4°C. The cleared sample was applied to two 5 ml of Ni-NTA cartridges (Qiagen). The column was washed in five steps (30 ml each) with lysis buffer supplemented with 5, 10, 15, 20, and 25 mM imidazole, and bound proteins were eluted with a linear gradient of 20 mM Tris–HCl (pH 7.5), 500 mM NaCl, 5% glycerol, and 500 mM imidazole in 50 ml (target buffer concentration 20%) followed by an elution step with 30 ml of lysis buffer supplemented with 100 mM imidazole. Elution fractions were pooled, concentrated using 30 000 molecular weight cut-off centrifugal filters (Merck Millipore), and further purified by size-exclusion chromatography using a HiLoad 16/600 Superdex 200 pg column (Cytiva) in 20 mM Tris–HCl (pH 7.5), 500 mM NaCl, 5% glycerol, and 1 mM DTT. The run resulted in a broad peak with a shoulder at a lower retention volume. Only the fractions corresponding to the main peak were concentrated and purified again by size-exclusion chromatography using a HiLoad 16/600 Superdex 200 pg column (Cytiva) in 20 mM Tris–HCl, pH 7.5, 500 mM NaCl, 5% glycerol, 1 mM DTT yielding pure, and monodisperse proteins. Purified His_6-MBP tagged $TnsAB^{CTD}$ was concentrated to 116 mg/ml using 3000 kDa molecular weight cut-off centrifugal filters (Merck Millipore) and flash-frozen in liquid nitrogen. The His_6-MBP tag on $TnsAB^{CTD}$ was intentionally left attached to use the protein as bait for TnsC pull-down experiments.

Analytical size-exclusion chromatography

To monitor TnsC heptamer formation, a 14-bp double-stranded DNA (dsDNA) (prepared by annealing Target3_f and Target3_r, Supplementary Table S2) was mixed with buffer, Milli-Q water, TnsC, and ATP to reach a final composition of 100 μM TnsC, 20 μM DNA, and 2 mM ATP in assembly buffer (20 mM Tris–HCl, pH 7.5, 500 mM NaCl, 10 mM $MgCl_2$, and 1 mM DTT), in a final volume of 25 μl. All analyzed samples contained $MgCl_2$ at a final concentration of 10 mM. For the samples without ATP, DNA, or TnsC, Milli-Q, annealing buffer (20 mM HEPES–KOH, pH 7.5, 100 mM KCl) or TnsC size exclusion buffer (20 mM Tris–HCl, pH 7.5, 500 mM NaCl, and 1 mM DTT) was used instead, respectively. The volume was incubated at 37°C for 40 min and centrifuged for 10 min at 4°C, 14 000 *g* before being injected in a Superdex 200 Increase 5/150 GL (Cytiva) using an ÄKTA pure Micro system (Cytiva) and assembly buffer as mobile phase. The same procedure was used to monitor TnsC oligomerization in the presence of ADP and/or DNA, for which a 25-bp dsDNA target was used (Target2_f and Target2_r, Supplementary Table S2).

To monitor TnsC heptamer disassembly, 20 μl of 124 μM TnsAB in assembly buffer supplemented with 1 mM ATP was added to a 25 μl of heptameric TnsC prepared as previously described. For the control sample without TnsAB, TnsAB size-exclusion buffer was used instead (20 mM Tris–HCl, pH 7.5, 500 mM NaCl, 5% glycerol, and 1 mM DTT). The mixture was incubated for 2 h at 4°C, centrifuged for 10 min at 4°C, 14 000 *g* before being injected in a Superdex 200 Increase 5/150 GL (Cytiva) using an ÄKTA pure Micro system (Cytiva) and assembly buffer as mobile phase. Fractions were analyzed by SDS–PAGE. To assess whether higher temperatures would influence the enzymatic activity and disassembly of the TnsC–TnsAB complex, additional size-exclusion chromatography (SEC) runs were conducted upon incubating TnsC–TnsAB at varying temperatures (25°C, 30°C, or 37°C) for 1 h.

To monitor TnsC disassembly in the absence of ATP excess, heptameric TnsC (100 μl) was prepared as described previously and injected in a Superdex 200 Increase 5/150 GL (Cytiva) using an ÄKTA pure Micro system (Cytiva) and assembly buffer as mobile phase. Fractions corresponding to the heptameric TnsC–DNA–ATP complex were pooled together resulting in 150 μl of prepurified TnsC heptamer at a protein concentration of 39 μM, measured with the Qubit Protein

Broad Range (BR) Assay Kit (Thermo Fisher). 71 µl of pre-purified TnsC heptamer were mixed with a 15 µl solution of TnsAB at 185 µM in assembly buffer, incubated at 4°C for 1 h, and centrifuged for 10 min at 4°C, 14 000 *g*, before being injected in a Superdex 200 Increase 5/150 GL (Cytiva) using an ÄKTA pure Micro system (Cytiva) and assembly buffer as mobile phase. Fractions were analyzed by SDS–PAGE.

Negative-stain electron microscopy

For TnsC heptamer visualization in the presence of DNA, ATP (Sigma–Aldrich), or ATP and DNA, TnsC was mixed with a dsDNA containing a 9-bp unpaired region at the centre and two 19-bp flanking paired regions, or with Milli-Q water. The target dsDNA was obtained by annealing two primers (Target1_f and Target1_r, Supplementary Table S2). All samples prepared for negative-stain electron microscopy contained $MgCl_2$ at a final concentration of 10 mM. After a 10-min incubation at room temperature, ATP or Milli-Q water was added, followed by a 20-min incubation at 37°C. The final sample contained 75 µM TnsC, 15 µM target DNA (0 µM in the case of the TnsC + ATP sample), and 1 mM ATP (0 mM in the case of the TnsC + DNA sample), 20 mM HEPES–KOH, pH 7.5, 200 mM KCl, 10 mM $MgCl_2$, and 1 mM DTT, in a final volume of 22 µl. The sample was 50-fold diluted with buffer before being used for grid preparation (final concentration: 1.5 µM).

For TnsC visualization in the presence of TnsAB, DNA, and ATP or AMPPNP (Sigma–Aldrich), the same procedure described before was followed, after which TnsAB was added in equimolar concentration, followed by a final incubation at 37°C for 10 min. The final sample contained 15 µM TnsC, 15 µM TnsAB, 3 µM target DNA, 1 mM ATP or AMPPNP, 20 mM HEPES–KOH, pH 7.5, 200 mM KCl, 10 mM $MgCl_2$, and 1 mM DTT, in a final volume of 15 µl. The sample was 20-fold diluted with buffer before being used for grid preparation (final concentration: 0.75 µM).

Samples (4 µl) were applied to glow-discharged continuous carbon film-supported copper grids (CF300-CU-50 grids, Electron Microscopy Sciences). After 1-min incubation, the grids were washed once with 4 µl of 2% (w/v) uranyl formate and stained in a 4-µl drop of 2% uranyl formate for 1 min before blotting. Negatively stained specimens were imaged using a FEI Tecnai G2 Spirit transmission electron microscope (University of Zurich) equipped with a LaB_6 electron source and operated at an acceleration voltage of 120 kV. Data were acquired at a nominal magnification of ×98 000 (TnsC–DNA sample, Fig. 1C) or ×120 000 (all the other images, Figs 1C and 4B) with a side-mounted Gatan Orius 1000 CCD camera (4 k × 2.6 k pixels, pixel size: 9 µm) and an exposure time of 0.5 s.

In vivo transposition assays and droplet digital PCR analysis

In vivo transposition experiments were conducted using *E. coli* BL21 Star (DE3) cells (Thermo Fisher Scientific). Cells were co-transformed with pDonor and pTarget_ΔtRNA plasmids (20 ng each), followed by isolation of transformants on Luria Broth (LB) agar plates containing two antibiotics (33 µg/ml of chloramphenicol and 100 µg/ml of ampicillin). A single colony from the plate was used to start liquid cultures, which were then processed to produce chemically competent strains through conventional methods, before being aliquoted and snap frozen. Competent cells were transformed with pHelper plasmids (300 ng) via heat shock. Cells were then allowed to recover in LB medium at 37°C for 1 h before being plated on LB-agar plates supplemented with three antibiotics (50 µg/ml of spectinomycin, 33 µg/ml of chloramphenicol, and 100 µg/ml of ampicillin) and incubated overnight at 37°C. Three colonies from each transformation were inoculated separately in 1 ml of LB media supplemented with the three antibiotics. The cultures were grown at 37°C for 3 h with shaking at 900 rpm. After growth, cell density of each culture was adjusted to $OD_{600} = 0.15$ by diluting with LB medium, and 300 µl of the cell suspension was plated on LB-agar plates supplemented with the same three antibiotics and 0.1 mM IPTG. After overnight growth at 30°C, colonies were harvested by resuspending in 1.5 ml LB medium and centrifuged for 3 min at 14 000 *g*. The cell pellet was then resuspended in 15 µl of lysis buffer (Tris–EDTA buffer with 0.1% Triton X-100) and 60 µl of Milli-Q water. The samples were heated for 5 min at 95°C and centrifuged for 10 min at 14000 *g*. The pellet was discarded and the supernatant was adjusted to 0.3 ng/µl of nucleic acid concentration.

The solution was used as a template DNA for ddPCR analysis. A reaction mixture containing five primers (900 nM) (ddPCR_primer1-5, Supplementary Table S2), two probes (250 nM) (ddPCR_probe1-2, Supplementary Table S2), 2.5 µl of template DNA (0.75 ng), and ddPCR Supermix for Probes (no dUTP) (1×) (BioRad) was prepared in a total volume of 20 µl. Droplets for PCR were formed using Droplet Generation Oil (70 µl) (Bio-Rad) in a QX200 Droplet Generator (BioRad). 40 µl of the final sample were transferred to 96-well plates for PCR amplification (1 cycle: 95°C, 10 min; 40 cycles: 94°C, 30 s, 52°C, 1 min; 1 cycle: 98°C, 10 min; 4°C hold). Samples were read out with a QX200 Droplet Reader (Bio-Rad) and analyzed with QuantaSoft software (Bio-Rad) to calculate the concentration of inserts and template DNA (Abs counting mode).

ddPCR_probe1 (5′-HEX/ZEN/3′-IBFQ) was designed to anneal to the transposon right end, while ddPCR_probe2 (5′-FAM/3′-BHQ1) annealed to the pTarget backbone. Upon successful transposition, ddPCR_primer2 and ddPCR_primer1 or 3, respectively, detecting left end to right end (LE–RE) or right end to left end (RE–LE) insertions, would amplify the region around ddPCR_probe1 and separate the HEX fluorophore from the quencher. The process was monitored by detecting the fluorescence signal in the HEX channel, thereby quantifying the number of pTarget plasmids which contained transposon DNA at the expected site. ddPCR_primer4-5 would amplify the pTarget backbone, which allowed quantification of the total number of pTarget plasmids by monitoring emission in the FAM channel. On-target transposition efficiencies were calculated using the formula: Efficiency (%) = [Copies of inserts/(Copies inserts + targets)]*100, based on data from three biological replicates, each measured in technical duplicates. No additional normalization was applied beyond this calculation. A positive control consisting of the pTarget plasmid in which the transposon DNA was cloned downstream of the protospacer adjacent motif (PAM) in the LE–RE orientation, mimicking a successful transposition event, was used to ensure that our method was able to detect transposition events. A schematic of the assay is shown in Supplementary Fig. S7.

Pull-down coprecipitation experiments

TnsC was mixed with a 25-bp dsDNA (obtained by annealing of two primers, Target2_f and Target2_r, Supplementary Table S2). After 10 min at room temperature, ADP, ATP, or AMPPNP (Sigma–Aldrich) was added to the sample, which was then incubated for 20 min at 37°C. The final sample contained 9 μM TnsC, 1.8 μM dsDNA, 1 mM ADP/AMPPNP/ATP, 20 mM HEPES–KOH, pH 7.5, 200 mM KCl, 10 mM $MgCl_2$, and 1 mM DTT, in a final volume of 118 μl. 34 μl of the sample, corresponding to 300 pmol TnsC, was mixed with 300 pmol of His-MBP-tagged TnsAB or $TnsAB^{CTD}$, and binding buffer (20 mM Tris–HCl, pH 7.5, 250 mM KCl, 1 mM DTT, 1 mM ADP/AMPPNP/ATP, and 0.1% Triton-X) was added to reach a total volume of 100 μl. The sample was incubated for 30 min at 4°C, after which 100 μl of binding buffer were added to the sample. After removing 20 μl of the sample as an input control, 50 μl of pre-equilibrated amylose resin (BioConcept) (50% suspension in binding buffer) was added. The mixture was incubated for 1 h at 4°C using a nutator. Afterward, beads were separated by centrifugation (2 min, 4°C, 500 *g*) and the supernatant was discarded. Four wash steps using 500 μl of binding buffer were performed. Beads were eluted with 25 μl of binding buffer supplemented with 10 mM maltose by mixing and incubating on ice for 10 min, followed by centrifugation (2 min, 4°C, 14000 *g*). 10 μl of input control and elution samples were loaded on an SDS–PAGE gel for each condition.

Cryo-EM sample preparation and data collection: TnsC–AMPPNP–dsDNA

Purified TnsC was mixed with a dsDNA containing a 9-bp unpaired region at the centre and two 19-bp flanking paired regions (obtained by annealing of the two primers Target1_f and Target1_r, Supplementary Table S2), AMPPNP, and buffer. The final sample contained 75 μM TnsC, 12.5 μM dsDNA, 1 mM AMPPNP, 20 mM HEPES–KOH, pH 7.5, 250 mM KCl, 10 mM $MgCl_2$, and 1 mM DTT, in a total volume of 22.4 μl. The volume was incubated at 37°C for 20 min and centrifuged at 14000 *g* for 10 min at 4°C. CHAPSO (0.8 mM final concentration) was added to the sample shortly before cryo-EM grid preparation to improve particle distribution. Without this additive, the particles tended to adopt a preferred orientation presenting primarily top views with the plane of the heptameric TnsC ring oriented parallel to the ice layer.

2.5 μl of the sample were applied to a freshly glow discharged 200-mesh Cu R1.2/1.3 grid with an ultrathin 2 nm continuous carbon (UTC) layer (commercially supplied by Quantifoil Micro Tools), blotted for 2.5 s at 100% humidity, 4°C, plunge frozen in liquid ethane (using a Vitrobot Mark IV plunger, FEI), and stored in liquid nitrogen. Carbon-coated grids were used to improve particle distribution, which was initially inadequate on unsupported grids. Cryo-EM data collection was performed on a FEI Titan Krios G3i microscope (University of Zurich, Switzerland) operated at 300 kV and equipped with a Gatan K3 direct electron detector in super-resolution counting mode. A total of 8036 movies were recorded at ×130 000 magnification, resulting in a super-resolution pixel size of 0.325 Å. Each movie comprised 37 subframes with a total dose of 59.172 $e^-/Å^2$. Data acquisition was performed with EPU Automated Data Acquisition Software for Single Particle Analysis (Thermo Fisher Scientific) with three shots per hole at −1.0 to −2.4 μm defocus (0.2 μm steps).

Cryo-EM data processing and model building: TnsC–AMPPNP–dsDNA

The collected exposures were processed in cryoSPARC (v4.0.1) [41]. Patch Motion Correction and Patch CTF Correction were used to align and correct the imported 8036 movies. To ensure that only the highest-quality data were used for downstream processing, movies with CTF fit resolution >5 Å were discarded using Curate Exposures, resulting in a total of 2321 accepted movies. Blob Picker (minimum particle diameter: 100 Å, maximum particle diameter: 150 Å, minimum separation distance: 0.5 diameters) was used to select particles (1 233 152 in total) which were included for further processing based on their NCC and power score, leading to 282 201 particles. Particles were extracted (extraction box size: 360 pixels; Fourier-cropped to box size: 120 pixels) and classified into 200 classes using 2D Classification. Twenty-two classes (41 951 particles) were selected, re-extracted with box size (480 pixels), and given as input to Ab-Initio Reconstruction and subsequently to Non-uniform Refinement. As the volume showed partial density and flexibility for one of the TnsC chains ($TnsC^G$), particles and mask were used as input for a 3D Variability Analysis, solving three modes and using 5 Å as filter resolution. The results were analyzed with 3D Variability Display in simple output mode with 20 frames. Two frames belonging to one mode were used as input for a 2-class Heterogeneous Refinement. After running a Non-uniform Refinement of both output volumes, one of them was used for a second round of 3D Variability Analysis, multi-class Heterogeneous Refinement, and Non-uniform Refinements as described above. The two outputs, together with the output volume of the first 3D Variability Analysis round, were used as inputs for a 3-class final Heterogeneous Refinement. The three volumes were refined with Non-uniform Refinement, leading to three densities corresponding to three states: a heptameric TnsC ring conformation (18 357 particles, 3.70 Å GSFSC resolution), a heptameric TnsC stretched-ring conformation (12 092 particles, 4.45 Å GSFSC resolution), and an octameric TnsC stretched-ring conformation (8979 particles, 4.47 Å GSFSC resolution). A detailed processing workflow is shown in the Supplementary Fig. S2. Refinement statistics are reported in Supplementary Table S1.

An initial model of PmcTnsC was generated using AlphaFold2 ColabFold [42, 43]. The model was manually docked as a rigid body in the cryo-EM density map corresponding to the heptameric ring conformation using UCSF ChimeraX [44], followed by real space fitting with the "Fit in Map" function. The model was subjected to manual refinement against the map using the software Coot [45] and real space refine in Phenix [46]. Secondary structure, side chain rotamer, Ramachandran, and nucleic acid restraints (base pair, stacking plane, and sugar pucker restraints calculated with the LibG script [47]) were used. The final model comprises seven copies of TnsC (residues 5–335 for chain 1 and 5–347 for chains 2–7), one copy of the target dsDNA [1–16], and seven AMPPNP molecules. Models for the low-resolution stretched-ring states were prepared following the same procedure. Structure and map figures were prepared using UCSF ChimeraX. Ring geometry analysis was performed using UCSF ChimeraX (using centroids for each chain as ref-

erences) and PyMol [48] (using the angle_between_domains function).

Cryo-EM sample preparation and data collection: TnsC–dsDNA–AMPPNP–TnsAB^{hook}

The TnsAB^{CTD}–TnsC complex was assembled and purified using a pull-down procedure as follows. Purified TnsC was mixed with a dsDNA containing a 9-bp unpaired region at the centre and two 19-bp based-paired flanking regions (obtained by annealing of the two primers Target1_f and Target1_r, Supplementary Table S2), AMPPNP, and buffer. The final sample contained 75 μM TnsC, 15 μM dsDNA, 1 mM AMPPNP, 20 mM HEPES–KOH, pH 7.5, 250 mM KCl, 10 mM $MgCl_2$, and 1 mM DTT in a total volume of 22.4 μl. The volume was incubated at 37°C for 20 min, after which 10.4 μl of purified MBP-tagged TnsB^{CTD} (231 μM) was added to the sample. The mixture was incubated at 37°C for 20 min, and 300 μl of amylose resin (BioConcept) (50% suspension equilibrated in 20 mM HEPES–KOH, pH 7.5, 250 mM KCl, 10 mM $MgCl_2$, and 1 mM DTT) was added. The sample was incubated for 2 h at 4°C using a nutator and centrifuged at 100 *g*, 4°C for 1 min. The resin was washed two times with 500 μl of wash buffer (20 mM HEPES–KOH, pH 7.5, 250 mM KCl, 10 mM $MgCl_2$, 1 mM DTT, and 1 mM AMPPNP), and 2 μl of His_6-TEV (74 μM) was added. The solution was incubated at 20°C for 1 h. Subsequently, the sample was centrifuged at 14 000 *g*, 4°C for 10 min. The supernatant was transferred and concentrated to ∼3 mg/ml using 100 kDa molecular weight cut-off centrifugal filters (Merck Millipore). CHAPSO (0.8 mM final concentration) was added to the sample shortly before cryo-EM grid preparation to improve particle orientation.

2.5 μl of the sample were applied to a freshly glow discharged 200-mesh Cu R1.2/1.3 grid with an ultrathin 2 nm continuous carbon (UTC) layer (commercially supplied by Quantifoil Micro Tools), blotted for 3.5 s at 100% humidity, 4 °C, plunge frozen in liquid ethane (using a Vitrobot Mark IV plunger, FEI), and stored in liquid nitrogen. Cryo-EM data collection was performed on a FEI Titan Krios G3i microscope (University of Zurich, Switzerland) operated at 300 kV and equipped with a Gatan K3 direct electron detector in super-resolution counting mode. A total of 11 134 movies were recorded at ×130 000 magnification, resulting in a super-resolution pixel size of 0.325 Å. Each movie comprised 42 subframes with a total dose of 60.480 $e^-/Å^2$. Data acquisition was performed with EPU Automated Data Acquisition Software for Single Particle Analysis (Thermo Fisher Scientific) with three shots per hole at −1.0 to −2.4 μm defocus (0.2-μm steps).

Cryo-EM data processing and model building: TnsC–AMPPNP–dsDNA–TnsB complex

The collected exposures were processed in cryoSPARC (v4.0.1) [41]. Patch Motion Correction and Patch CTF Correction were used to align and correct the imported 11 134 movies. Blob Picker (minimum particle diameter: 120 Å and maximum particle diameter: 200 Å) was used to select particles (3 376 428 in total), which were included for further processing based on their NCC and power score, leading to 711 461 particles. Particles were extracted (extraction box size: 480 pixels; Fourier-cropped to box size: 120 pixels) and classified into 100 classes using 2D Classification. Four classes (29 559 particles) were selected and given as input to a 2-class Ab-Initio Reconstruction. Particles and volumes of one of the two Ab-Initio classes were used as input for Non-uniform Refinement after particle re-extraction (extraction box size: 480 pixels), leading to a 3.22 Å volume (GSFSC resolution). A detailed processing workflow is shown in the Supplementary Fig. S9. Refinement statistics are reported in Supplementary Table S1.

The TnsC–AMPPNP–DNA ring model was manually docked as rigid body in the TnsC–AMPPNP–dsDNA–TnsAB^{hook} cryoEM density map using UCSF ChimeraX [44], followed by real space fitting with the "Fit in Map" function. Additional density was observed in the proximity of six copies of TnsC. The model was built and subjected to manual refinement against the map using the software Coot [45] and real space refine in Phenix [46]. Secondary structure, side chain rotamer, Ramachandran, and nucleic acid restraints (base pair, stacking plane, and sugar pucker restraints calculated with the LibG script [47]) were used. The final model comprises seven copies of TnsC (residues 5–337 for chain 1 and 5–347 for chains 2–7), one copy of the target dsDNA [1–16], six copies of TnsAB hook (residues 892–898), and seven AMPPNP molecules.

In vitro ATP hydrolysis assay

ATP hydrolysis was measured using a Malachite Green Phosphate assay (Sigma–Aldrich), following the protocol reported in [26]. TnsC (7.5 μM) was incubated for 2 h at 4°C or for 1 h at 22°C with a 14-bp dsDNA (7.5 μM) prepared by annealing Target3_f and Target3_r oligonucleotides (Supplementary Table S2), ATP (1 mM), and TnsAB (15 μM) in a volume of 5 μl (final buffer: 20 mM HEPES, pH 7.5, 2 mM $MgCl_2$, 180 mM NaCl, 10 μM $ZnCl_2$, and 1 mM DTT). A positive control sample containing type V-K CAST ShTnsC (7.5 μM), a 92-bp dsDNA (7.5 μM) prepared by annealing Target_V-K_f and Target_V-K_r oligonucleotides (Supplementary Table S2), ATP (1 mM), and ShTnsB (15 μM) in a final 5 μl volume was prepared and incubated for 2 h at 4°C or for 1 h at 22°C (Fig. 4C). Additionally, the same PmCAST samples were prepared with the buffer and conditions used for monitoring assembly by SEC (2 h at 4°C; final buffer: 20 mM Tris–HCl, pH 7.5, 500 mM NaCl, 10 mM $MgCl_2$, and 1 mM DTT) (Supplementary Fig. S12). For samples without TnsC or TnsAB, their respective storage buffers were used instead. The samples were diluted with 40 μl of water and incubated with 10 μl of the working reagent for 5 min, after which the absorbance at 620 nm was measured in a 96-well UV-transparent microplate (Corning) using a PHERAstar FSX Reader (BMG LabTech). All samples were blank corrected. Each reaction was prepared in three independent replicates, each measured in duplicates.

Results

Type I-B CAST TnsC assembles into a pseudosymmetric heptamer

The type I-B subtype 2 (I-B2) CAST system from *Peltigera membranacea cyanobiont 210A* (Pmc) encodes TnsC along with the TnsAB transposase fusion protein, as well as TniQ and TnsD proteins [14, 15], which were previously shown to be required for RNA-targeted transposition or homing downstream of tRNA genes, respectively [19] (Fig. 1A). The

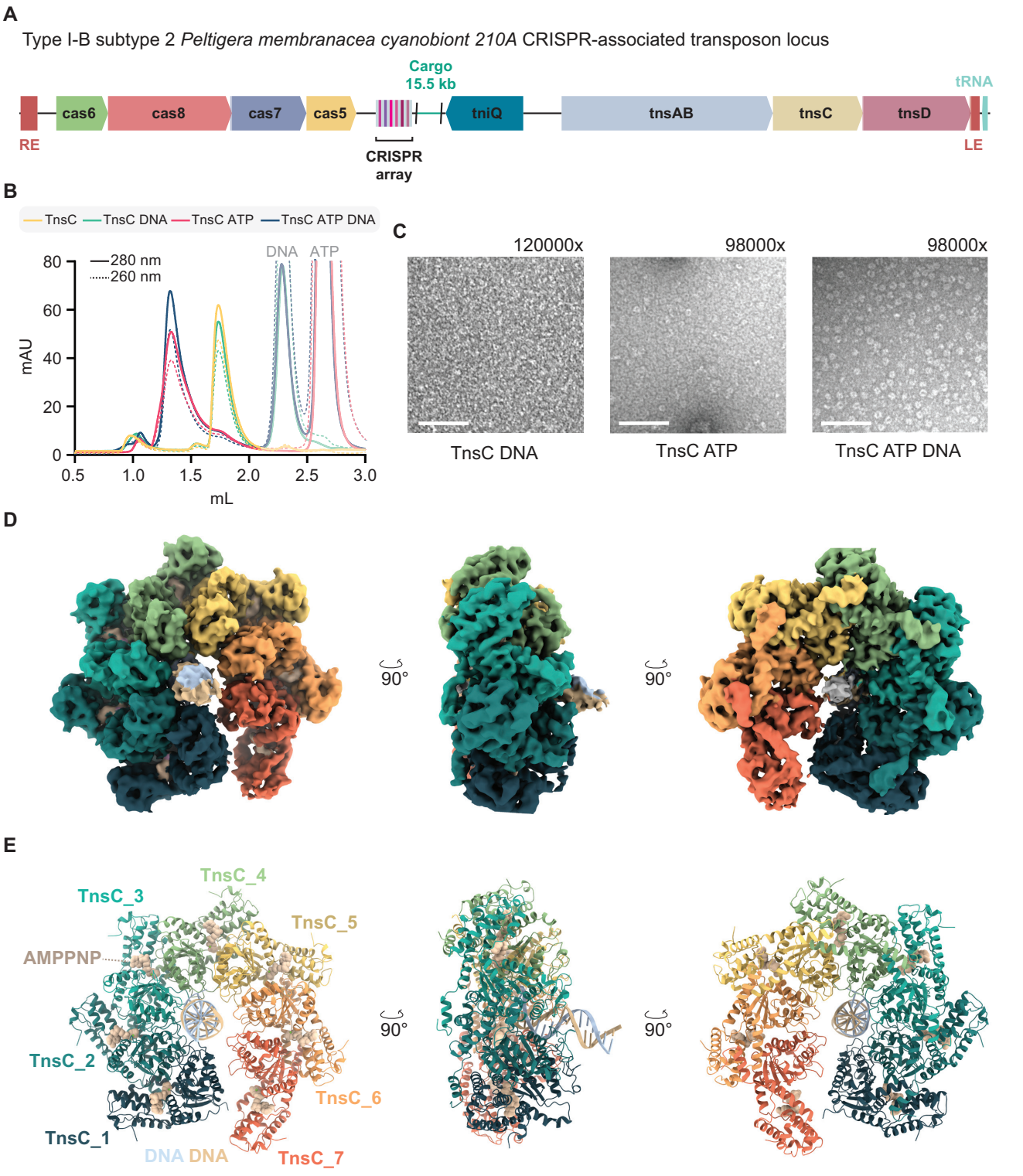

Figure 1. PmcCAST TnsC forms a heptameric complex in the presence of ATP and DNA. (**A**) Schematic representation of the type I-B CAST system from *Peltigera membranacea cyanobiont 210A*. LE and RE denote left and right transposon ends. (**B**) Size-exclusion chromatography profiles of TnsC alone, in the presence of ATP, double-stranded (ds)DNA, or both ATP and dsDNA. (**C**) Representative negative-stain electron micrographs of TnsC in the presence or absence of dsDNA and/or ATP. Scale bar corresponds to 100 nm. (**D**) Single-particle cryo-EM reconstruction of the dsDNA- and AMPPNP-bound TnsC heptamer (from left to right: top, side and bottom views). (**E**) Structural model of the dsDNA- and AMPPNP-bound TnsC heptamer (from left to right: top, side and bottom views). Individual TnsC protomers are labeled with distinct superscript letters to differentiate each subunit. AMPPNP molecules are shown in space-fill representation.

PmcTnsC protein contains an "ATPases Associated with diverse cellular Activities" (AAA+) ATPase domain [49] and shares 17% sequence identity with canonical Tn7 TnsC (HHpred [50] probability 99.79%). As AAA+ ATPases typically couple nucleotide binding with higher-order oligomer formation [51], we investigated PmcTnsC oligomerization in the presence of ATP and/or double-stranded DNA. Consistent with recent findings [37], size-exclusion chromatography analysis indicated that PmcTnsC forms higher-molecular weight species in the presence of ATP, with or without dsDNA (Fig. 1B and Supplementary Fig. S1A). These results were corroborated by the observation of ring-like oligomers by negative-stain electron microscopy (Fig. 1C). Ring formation was not observed in the presence of dsDNA only (Fig. 1B and C), and neither ADP alone nor ADP together with dsDNA was found to induce oligomerization (Supplementary Fig. S1B).

To gain structural insights into the self-assembly mechanism, we determined the cryo-EM structure of PmcTnsC in the presence of the non-hydrolyzable ATP analog AMPPNP and a dsDNA substrate at a resolution of 3.7 Å (Fig. 1D; Supplementary Fig. S2 and Supplementary Table S1). The structure reveals that TnsC forms a domed heptameric ring assembled around a DNA duplex inserted in the hollow ring cavity (Fig. 1E). While the bound DNA adopts near-perfect B-form duplex geometry, the heptameric PmcTnsC ring is open due to the presence of a gap between the first ($TnsC^{A}$) and last ($TnsC^{G}$) protomers, breaking the seven-fold symmetry (Fig. 1E and Supplementary Fig. S3). As a result of the symmetry mismatch, the TnsC protomers are asymmetrically positioned with respect to the DNA, with the first four protomers ($TnsC^{A}$, $TnsC^{B}$, $TnsC^{C}$, and $TnsC^{D}$; Supplementary Fig. S3A) establishing direct physical contacts with the DNA backbone, in contrast to the last three TnsC protomers ($TnsC^{E}$, $TnsC^{F}$, and $TnsC^{G}$; Supplementary Fig. S3A and B), which do not interact with the nucleic acid. The cryo-EM density for the DNA bases is averaged out, likely due to sequence-unspecific binding to the TnsC protomers (Fig. 1D). All seven ATPase active site clefts located at the interfaces between the AAA + domains of TnsC protomers within the ring are occupied by AMPPNP molecules (Fig. 1D and E).

The TnsC AAA + domain is composed of an N-terminal α/β core (residues 31–117 and 164–229) and a C-terminal α-helical bundle (residues 230–308), together comprising the typical bilobed ATPase fold [51] (Supplementary Fig. S4A and B). Inserted within the α/β core is the initiator-specific motif (ISM, residues 130–163), a DNA-binding motif characteristic of the AAA + ATPase initiator clade [51], and an insertion motif (residues 118–129), which has been shown to interact with TniQ [37] (Supplementary Fig. S4A and B). The two motifs decorate the inner rim of the ring, while the N-terminal helices (residues 5–30) form its outer edge (Supplementary Fig. S4C). The concave face of the ring is formed by the C-terminal helices (residues 309–347) which connect neighboring TnsC protomers (Supplementary Fig. S4D). The C-terminal segments of TnsC (residues 348–383) are not visible in the cryo-EM density map, likely due to structural disorder. Further processing of the cryo-EM data yielded two additional low-resolution (~4.5 Å) reconstructions of heptameric and octameric TnsC complexes with expanded central cavities in which two DNA molecules are bound simultaneously (Supplementary Fig. S5 and Supplementary Table S1). Although these structures indicate considerable intrinsic dynamics of the PmcTnsC oligomeric assemblies, they likely represent *in vitro* artifacts that do not seem to have biological relevance.

A recently reported structure of DNA-bound TnsC reconstituted in the presence of ATP (PDB: 8FCW) revealed considerable structural heterogeneity, with only five TnsC copies resolved in the reconstruction [37]. In contrast, our structural data indicate that TnsC is able to assemble into a stable heptamer in the presence of a nonhydrolyzable ATP analog. Structural overlays of the AMPPNP-reconstituted PmcTnsC heptamer with the PmcCascade–TniQ–TnsC complex (PDB: 8FF4) reveal only minor conformational differences between individual PmcTnsC protomers (Supplementary Fig. S6A and B), restricted mostly to the two protomers at the ring seam that interact with TniQ (Supplementary Fig. S6C and D). Taken together, these findings indicate that PmcTnsC is able to assemble into a heptameric ring in the absence of the target selector module (Cascade–TniQ complex or TnsD) and that the assembly of the TnsC heptamer is maintained upon interactions with the target selector and transposase components of the PmcCAST system.

TnsC oligomerization, ATPase activity, and DNA binding are required for CAST activity

AAA + ATPases are members of the P-loop protein superfamily [52] and thus contain so-called Walker-A and Walker-B motifs that are critical for ATP binding and hydrolysis [52–55]. The corresponding motifs in PmcTnsC, ^{57}GASGVGKT^{64} (Walker A), and ^{167}VFFVDE^{172} (Walker B) coordinate the AMPPNP ligands in the PmcTnsC–AMPPNP–DNA complex (Fig. 2A and B). Specifically, Lys63, Thr64, and Glu172 interact with the AMPPNP β- and γ-phosphate groups, and Thr64 additionally participates in the octahedral coordination of a Mg^{2+} cation (Fig. 2B). As in other P-loop ATPases, the C-terminal glutamate in the Walker B motif of PmcTnsC (Glu172) is positioned to activate a water molecule for nucleophilic attack on the γ-phosphate of ATP [51, 56], suggesting that PmcTnsC is capable of catalyzing ATP hydrolysis. In most AAA+ ATPases, this conserved glutamate switches from an active to an inactive conformation upon ATP binding [57, 58] and its mutation abolishes ATP hydrolysis without affecting ATP binding. Two arginine finger residues, Arg223 and Arg224, provided by a neighboring TnsC protomer in *trans*, complete the active site, thereby coupling ATP binding to TnsC oligomerization.

To probe the functional importance of the ATPase active site residues for the transposition activity of PmcCAST, we used a plasmid-based transposition activity assay in *E. coli*, quantifying the transposition efficiency using droplet digital PCR (ddPCR) (Supplementary Fig. S7). Cotransformation of donor and target plasmids together with a helper plasmid expressing WT PmcCAST resulted in detectable transposition in ~13% of cells. In contrast, cotransformation with a helper plasmid harboring mutations corresponding to alanine substitutions of Lys63, Glu172, or Arg224 in TnsC did not result in detectable transposition, indicating that both ATP binding and hydrolysis by TnsC are required for efficient targeted transposition activity in the PmcCAST system (Fig. 2C).

Besides the arginine finger residues, three additional electrostatically complementary interfaces facilitate PmcTnsC interprotomer contacts (Fig. 2A and D–F). Adjacent to the nucleotide binding pocket, Glu100, Glu108, and Arg112 in one protomer interact with Arg153, Arg154, and Glu157,

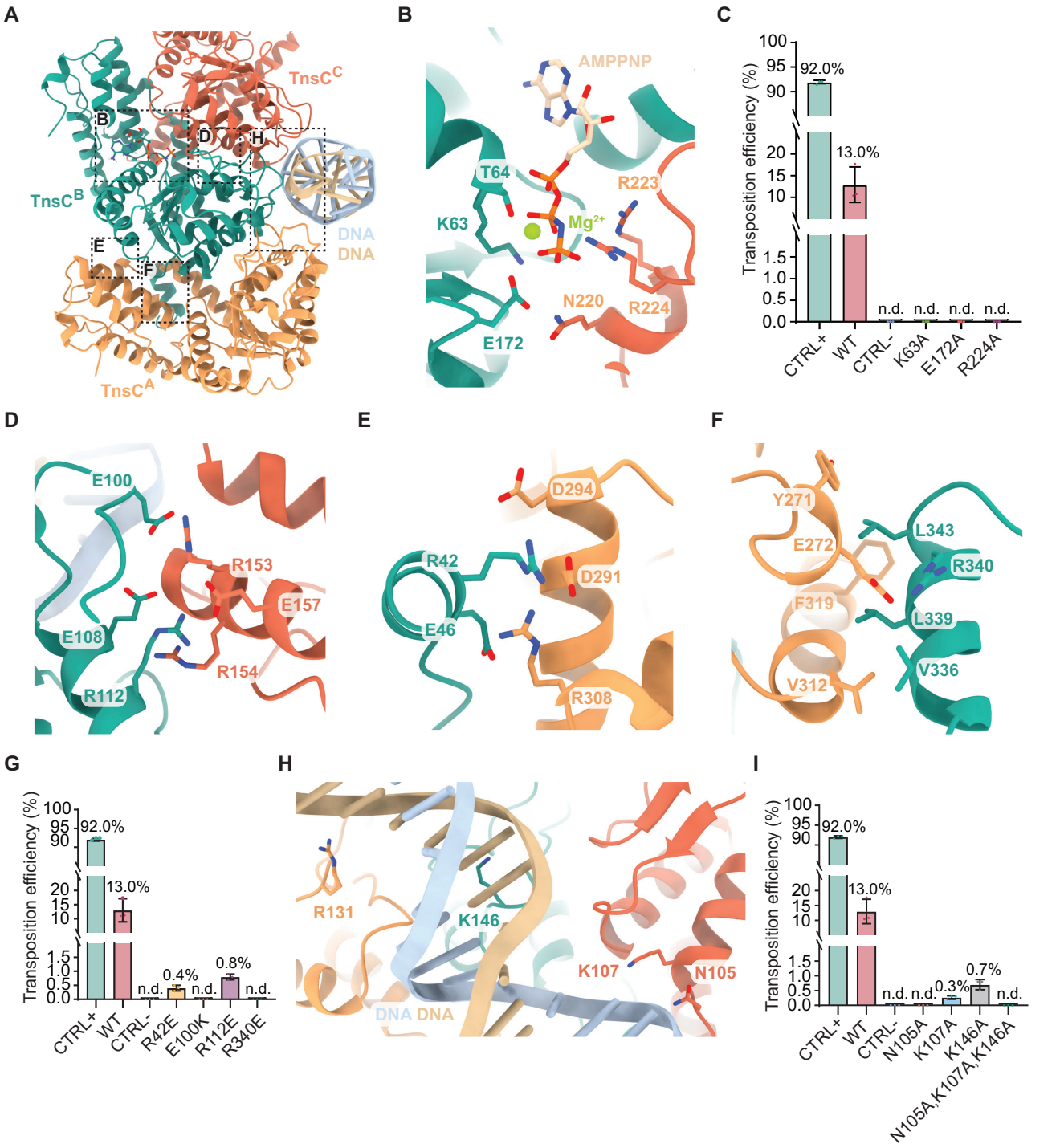

Figure 2. TnsC oligomerization, DNA binding and ATP hydrolysis are required for transposition. (**A**) Inter-protomer interfaces within the TnsC heptamer. Regions depicted in detail in subsequent panels are indicated with dashed boxes. (**B**) Detailed view of the ATPase catalytic pocket. Bound AMPPNP and interacting amino acid residues are shown in stick format. Mg^{2+} ion is depicted as a green sphere. (**C**) RNA-guided transposition activity in *E. coli* of PmcCAST systems containing mutations in the catalytic pocket of TnsC, as quantified by ddPCR. Data are presented as mean ± s.d. of three biologically independent replicates ($n = 3$), each measured in technical duplicates. Bars labeled as n.d. ("non-detectable") indicate values below the detection limit of the assay. The positive control ("CTRL+") corresponds to a ddPCR reaction that uses as DNA template an artificial pTarget plasmid with the transposon DNA from the pDonor plasmid inserted at the target site in the left end–right end (LE–RE) orientation. (**D**–**F**) Detailed views of the TnsC inter-protomer interfaces. (**G**) RNA-guided transposition efficiency in *E. coli* of PmcCAST systems containing mutations in the inter-protomer interfaces, quantified by ddPCR as in panel (C). (**H**) Detailed view of the DNA-binding interfaces. Only residues within 3.5 Å of the DNA are displayed. (**I**) RNA-guided transposition efficiency in *E. coli* of PmcCAST systems containing mutations in the DNA-binding interfaces, quantified by ddPCR as in panel (C).

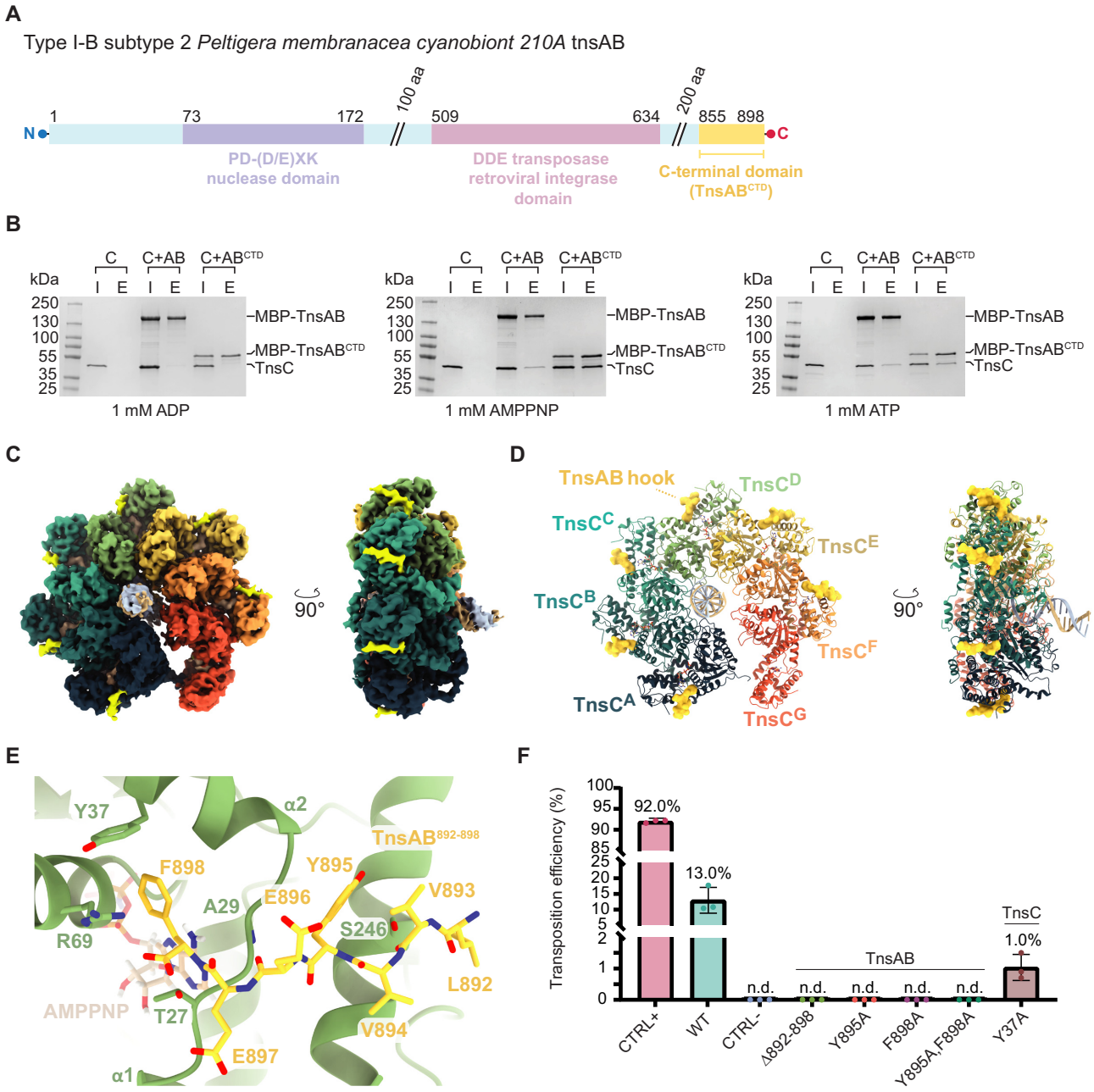

Figure 3. The C-terminal hook in TnsAB interacts with heptameric TnsC. (**A**) Schematic diagram of the domain organization of type I-B PmcCAST TnsAB. (**B**) Coprecipitation of TnsC by amylose-immobilized TnsAB (full-length or C-terminal domain), fused to MBP) in the presence of different nucleotides (ADP, AMPPNP, ATP; bottom). I: 10% input; E: elution; C: TnsC-only control; C + AB: TnsC and MBP-TnsAB full-length sample; C + AB^{CTD}: TnsC and MBP-TnsAB C-terminal domain sample. (**C**) Single-particle cryo-EM reconstruction of the heptameric TnsC–DNA–AMPPNP complex bound to six copies of the TnsAB hook (top and side views). Individual TnsC subunits are indicated with different colours. The TnsAB hooks densities are depicted in bright yellow. (**D**) Structural model of the TnsC–DNA–AMPPNP complex bound to six copies of the TnsAB hook (top and side views). Individual TnsC protomers are labeled with distinct superscript letters to differentiate each subunit. The TnsAB hooks are depicted in space-fill representation (bright yellow). (**E**) Detailed view of the TnsAB hook and the TnsC interface. (**F**) RNA-guided transposition activity in *E. coli* of PmcCAST systems containing mutations in the TnsAB hook and TnsC interface, as quantified by ddPCR. Data are presented as mean ± s.d. of three biologically independent replicates ($n = 3$), each measured in technical duplicates. Bars labeled n.d. ("non-detectable") indicate values below the detection limit of the assay. The positive control ("CTRL+") corresponds to a ddPCR reaction that uses as DNA template an artificial pTarget plasmid with the transposon DNA from the pDonor plasmid inserted at the target site in the left end-right end (LE–RE) orientation.

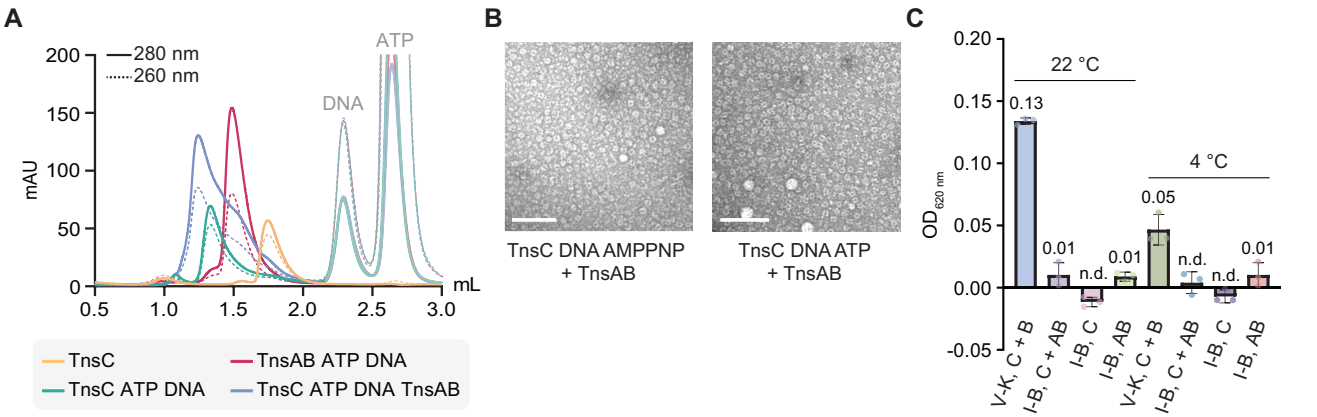

Figure 4. TnsAB does not induce ATPase activity and disassembly of heptameric TnsC. (**A**) Size-exclusion profiles of TnsC alone or in the presence of ATP/dsDNA or ATP/dsDNA and TnsAB. (**B**) Representative negative-stain electron micrographs of TnsC in the presence of dsDNA, TnsAB, and ATP or AMPPNP. Scale bar corresponds to 100 nm. (**C**) ATPase activity of PmcTnsAB (C + AB), PmcTnsC (**C**), or PmcTnsAB (AB) at 22°C and 4°C, as measured using a Malachite Green phosphate assay. Type V-K ShTnsC with ShTnsB was used as a positive control. All samples contain dsDNA and ATP. Data are presented as mean ± s.d. of three independent replicates ($n = 3$), each measured in technical duplicates. Bars labeled n.d. ("non-detectable") indicate values below the detection limit of the assay.

respectively, in the other (Fig. 2D). A second inter-protomer interface is formed by salt-bridge contacts between the residues Asp291, Asp294, and Arg308 in the α-helical AAA+ lid and Arg42, Glu46 in the N-terminal region of the α/β core (Fig. 2E). The final interface involves an α-helical motif (residues 329–347) in the C-terminal region, which projects over the α-helical AAA+ lid domain of the neighboring protomer and is anchored by hydrophobic interactions and a salt bridge between Arg340 and Glu272 (Fig. 2F and Supplementary Fig. S4D). Charge-reversal mutations at all three interfaces resulted in severe reduction or complete loss of transposition activity of PmcCAST in *E. coli* (Fig. 2G), underscoring the functional importance of TnsC oligomerization for the transposition mechanism of Type I-B CAST systems.

Within the heptameric ring, the bound DNA duplex is engaged via electrostatic interactions with the positively charged residues Lys107 (in protomers $TnsC^{C}$ and $TnsC^{D}$), Arg131 ($TnsC^{A}$), Lys146 ($TnsC^{B}$ and $TnsC^{E}$), and by a hydrogen bonding contact with Asn105 of $TnsC^{C}$ (Fig. 2H). In agreement, alanine substitutions of Lys107 and Lys146 substantially impaired transposition *in vivo*, while mutation of Asn105 reduced *in vivo* transposition below the limit of detection (Fig. 2I). Altogether, the mutational analysis of the main interaction interfaces of the TnsC–AMPPNP–DNA complex confirms the importance of oligomeric ring assembly, ATP hydrolysis, and DNA binding by TnsC for transposition of type I-B CAST systems *in vivo*.

The C-terminal hook of TnsAB interacts with heptameric TnsC

In the PmcCAST system, the transposase TnsAB is a natural fusion of TnsA and TnsB, comprising a PD-(D/E)XK nuclease (residues 73–172) and a DDE-motif transposase/integrase (residues 509–634) domains responsible for generating the 5′ and 3′ termini, respectively, at the transposon ends (Fig. 3A). The C-terminal segment of PmcTnsAB, spanning residues 855–898 (hereafter referred to as $TnsAB^{CTD}$), is predicted to be intrinsically unstructured, based on structural disorder predictions using DISOPRED3 [59] and an AlphaFold2 [42, 43] model of PmcTnsAB (Supplementary Fig. S8). This evokes similarities with the C-terminal regions of the canonical *E. coli* Tn7 TnsB [60] and type V-K CAST ShTnsB [30]. In these systems, the C-terminal unstructured regions of TnsB have been shown to interact with TnsC [12, 30, 32, 33, 60, 61] and stimulate the ATPase activity of TnsC [60]. To investigate the functional role of PmcTnsAB and its C-terminal segment in interactions with PmcTnsC, we performed coprecipitation (pull-down) experiments using recombinantly expressed, purified PmcTnsAB and the standalone C-terminal segment. PmcTnsC was not coprecipitated by full-length PmcTnsAB or $PmcTnsAB^{CTD}$ in the presence of ADP (Fig. 3B). In contrast, both full-length PmcTnsAB and $PmcTnsAB^{CTD}$ coprecipitated PmcTnsC in the presence of ATP or AMPPNP, with a stronger effect observed in the presence of AMPPNP. This indicates that the C-terminal segment of PmcTnsAB is alone sufficient to mediate interaction with PmcTnsC and that TnsAB interacts with TnsC specifically in its ATP-dependent oligomerized state.

Given the previously documented essential role of the TnsB C-terminal segment in Tn7 [12, 60, 61] and type V CAST [30, 32, 33] systems, we sought to identify the specific molecular determinants underpinning the interaction between $PmcTnsAB^{CTD}$ and the TnsC heptamer. To this end, we reconstituted a $PmcTnsAB^{CTD}$–TnsC–DNA–AMPPNP complex by affinity co-purification and subjected it to cryo-EM single-particle analysis (Fig. 3C; Supplementary Fig. S9 and Supplementary Table S1). The resulting structure, determined at a resolution of 3.2 Å, closely matches that of the TnsC–DNA–AMPPNP complex, revealing additional densities located at the junctions between the α/β AAA+ core and the α-helical lid domain of six TnsC subunits ($TnsC^{A}$, $TnsC^{B}$, $TnsC^{C}$, $TnsC^{D}$, $TnsC^{E}$, and $TnsC^{F}$; Fig. 3C and D). Based on density features characteristic of aromatic side chains, we were able to model the last seven residues of the PmcTnsAB C-terminal tail (residues 892–898), hereafter termed the TnsAB hook based on analogies with the type V TnsB [30] (Fig. 3D and E). This is consistent with a recently reported cryo-EM structure of the PmcTnsABCD complex, in which TnsC was also observed to interact with the C-terminal residues of PmcTnsAB [62].

The PmcTnsAB hook is bound at the interface of the two TnsC core domains in close proximity to the nucleotide binding pocket. However, it does not directly contact the bound AMPPNP molecule. The hook is anchored within the TnsC heptamer through a network of intermolecular backbone hydrogen-bonding interactions involving TnsAB residues of Val893, Glu896, and Phe898 and TnsC residues Ser246, Ala29, and Thr27 (Fig. 3E). TnsAB Tyr895 is inserted in a pocket at the base of the turn between the TnsC helices α1 and α2, while TnsAB Phe898 and TnsC Tyr37 engage in perpendicular (T-shaped) π–π interaction (Fig. 3E). Finally, TnsC Arg69 forms a salt bridge with the C-terminal carboxyl group of the hook (Fig. 3E). Truncation of the PmcTnsAB hook at residue Thr891 or alanine substitutions of the aromatic residues within the hook led to complete loss of transposition of PmcCAST *in vivo*, while alanine substitution of TnsC Tyr37 led to a substantial reduction, confirming the functional importance of the TnsC–TnsAB hook interaction (Fig. 3F). Taken together, these results confirm the essential role of the TnsAB C-terminal segment for the transposition activity of I-B CASTs, mirroring its importance in other related systems.

TnsAB does not induce TnsC oligomer disassembly in type I-B CAST systems

In the type V-K CAST system, the interaction of TnsB with polymeric TnsC filaments induces filament disassembly by stimulating the ATPase activity of TnsC [27, 30, 32]. To test whether type I-B CASTs use a similar mechanism, we monitored using analytical size-exclusion chromatography the oligomeric state of PmcTnsC, preassembled on dsDNA in the presence of ATP and 10 mM Mg^{2+}, following incubation with PmcTnsAB (Fig. 4A and Supplementary Fig. S10). Addition of PmcTnsAB to PmcTnsC in the presence of dsDNA and ATP resulted in a shift to a lower retention volume, indicating that PmcTnsAB interacts with the PmcTnsC heptamer without inducing its disassembly. Although increasing incubation temperatures impacted TnsAB solubility, comparable elution profiles were obtained when the TnsAB–TnsC incubations were performed at 4, 25, and 30°C, without detectable indication of heptamer disassembly (Supplementary Fig. S11A–E). Similar results were observed when the TnsC–DNA–ATP complex was pre-purified to remove excess ATP used to induce initial TnsC assembly (Supplementary Fig. S11F–J), indicating that the persistence of the heptameric PmcTnsAB–PmcTnsC complex is not due to repeated cycles of TnsC dissociation and reassembly. Validating these results, we used negative-stain electron microscopy to observe DNA-dependent formation of PmcTnsC oligomeric rings in the presence of PmcTnsAB, $MgCl_2$, and ATP or AMPPNP (Fig. 4B).

In the canonical *E. coli* Tn7 transposon, substituting ATP with AMPPNP abolishes target specificity and immunity, indicating that ATP hydrolysis is essential for these processes [63, 64]. In order to investigate the ATPase activity of PmcTnsC, we monitored ATP hydrolysis by PmcTnsC alone or PmcTnsC–TnsAB in the presence of dsDNA and $MgCl_2$ (Fig. 4C and Supplementary Fig. S12). As a positive control, we used TnsC from the type V-K ShCAST system (ShTnsC), whose ATPase activity has been shown to be activated by ShTnsB [26, 32]. PmcTnsC did not exhibit detectable ATPase activity on its own, nor in the presence of PmcTnsAB (Fig. 4C and Supplementary Fig. S12). In contrast, ShTnsC–TnsB exhibited substantial ATP turnover. Taken together, these findings indicate that, unlike in type V CASTs, TnsC oligomers do not undergo disassembly upon interaction with the TnsAB transposase in type I-B systems, nor is the ATPase activity of TnsC stimulated upon interaction with TnsAB.

Discussion

TnsC multimerization in CAST systems

In CAST systems, RNA-guided transposition depends on the effective communication between the CRISPR–Cas targeting complex and the transposase enzymatic machinery. These molecular interactions rely on the formation of multimeric TnsC complexes with distinct functional interfaces. TnsC assembly is itself coupled to ATP and target DNA binding and results in the formation of a polymeric filament in type V CAST systems, while type I-B and I-F TnsC proteins form heptameric ring-like assemblies, as shown by our work and other studies [27, 28, 37, 38, 62]. Despite differences in their overall (sub)domain architectures, TnsC proteins exhibit similar structural features in their overall folds (Supplementary Fig. S13A) and oligomerization interfaces (Supplementary Fig. S13B). In type I-B and type V TnsC complexes, the ISM and insertion subdomains are located on the convex face of the heptameric ring or the corresponding N-terminal face of the polymeric filament, respectively, and are involved in the interaction with the CRISPR targeting module [29, 37], while the lateral surface interacts with the TnsB C-terminal hooks [30, 32, 33]. In type V CAST, the TnsB IIβ domain interacts with the concave C-terminal face of the filament [32, 33] and a similar binding mode has recently been observed in the structure of the type I-B PmcCAST TnsABCD holocomplex [62]. Type I-B TnsC possesses a C-terminal region comprising an α-helical domain followed by an intrinsically disordered tail, while type I-F TnsC has a shorter C-terminal region (53 versus 73 amino acid residues) and type V TnsC lacks it altogether (Supplementary Fig. S13A). The C-terminal region of type I-B TnsC is positioned at the concave face of the TnsC ring (Supplementary Fig. S4D and Supplementary Fig. S13B), creating a TnsAB-interacting interface that is structurally distinct from the type V CAST. The C-terminal domain of type I-B TnsC is further involved in essential interprotomer interactions within the ring and can be observed connecting the two TnsC protomers at the seam of the TnsC ring in the TnsAB hook-bound structure, thereby closing the gap. Thus, the complex structural interplay of TnsC (sub)domains modulates its self-assembly properties and consequently defines the oligomer architecture. This in turn may have functional implications for distinct aspects of the transposition mechanism in specific CAST subtypes, including TnsC nucleation and oligomerization, target DNA remodeling, as well as transpososome recruitment and disassembly. Recent structural and biochemical analysis of the canonical *E. coli* Tn7 TnsC and its interactions with the target selector protein TnsD reveals that TnsD promotes stepwise assembly of the TnsC heptamer by acting as a nucleotide exchange factor [65]. Whether Cascade and TniQ fulfil a similar role in the RNA-guided transposition mechanism of type I CAST systems remains to be investigated.

Transposase recruitment by the TnsC–TnsAB hook interaction

Our study reveals that type I-B TnsAB interacts with the TnsC heptamer using a C-terminal hook motif comprising

seven residues and that this interaction is critical for transposition activity. In type V CASTs, TnsB binds the TnsC filament through an equivalent 14-residue motif at its C-terminus [30, 32, 33], with four TnsB hooks of the TnsB tetramer bound to the TnsC filament, and additional interactions between the IIβ and C-terminal domains of one TnsB protomer with the TnsC filament C-terminal face [32, 33] (Supplementary Fig. S14A–C). Although the PmcTnsC heptamer can bind up to six copies of the TnsAB hook, the recent structure of the PmcCAST TnsABCD complex revealed that transpososome assembly involves the binding of four hook motifs to the TnsC heptamer [62], in analogy with the type V CAST systems and agreement with the conserved tetrameric architecture of TnsB. Notably, one of the TnsAB binding sites in the TnsC heptamer (that of protomer $TnsC^{A}$) is occupied by the N-terminal domain TniQ in the context of the type I-B Cascade–TniQ–TnsC transposon recruitment complex [37] (Supplementary Fig. S14D), implying that only five sites are available for TnsAB recruitment upon Cascade/TniQ-mediated TnsC assembly at the target site.

The structural superposition of TnsAB hook-bound TnsC complexes from type I-B and type V systems reveals that the TnsC interface mediating the hook coordination is conserved (Supplementary Fig. S14A–C). In both CAST systems, the TnsAB/B hook motifs are positioned in a cleft formed by the α/β- and α-helical TnsC domains, near the nucleotide binding site (Supplementary Fig. S14A–C). However, compared to the type I-B interaction, the C-terminus of the type V TnsB hook is shifted ∼20 Å away from the C-terminal face of the filament and is more deeply inserted into the V-shaped cavity formed by the TnsC subdomains, in proximity of the ATP pocket (Supplementary Fig. S14C). Although the precise mechanism underlying TnsB-stimulated activation of TnsC ATPase and consequent filament disassembly remains elusive, both the hook and the additional TnsC-interacting regions of TnsB are essential for this process [32]. It is tempting to speculate that the different positioning of the transposase hook in type I-B CAST explains the inability of TnsAB to trigger ATP hydrolysis. However, further investigations will be necessary to clarify the mechanisms coupling transposase recruitment and TnsC disassembly in distinct CAST systems. Our results indicate that type I-B TnsAB does not stimulate TnsC heptamer disassembly *in vitro*, a striking difference from the type V CASTs. Although it is conceivable that TnsAB-induced TnsC oligomer disassembly might occur only when TnsC is assembled together with the target selector modules of type I-B CASTs, namely Cascade-TniQ or TnsD, recently reported structures of target-bound PmcCAST complexes containing either Cascade-TniQ [37], or TnsD and TnsAB [62], in which TnsC heptamerization is preserved, suggest that this is not the case. Type I CAST systems mediate RNA-guided transposon insertion at a site located 83–92 bp downstream from the protospacer-adjacent motif (PAM) sequence [19, 37]. With a footprint of ∼85 bp on the target DNA, as based on structural modeling and recently determined experimental structures [37, 62], the persistence of a stable TnsC heptamer bridging the Cascade-TniQ targeting module and the TnsAB transpososome thus provides a molecular ruler mechanism for defining the position of the transposon insertion site relative to the target binding site (Supplementary Fig. S14E).

Functional role of TnsC ATPase activity in type I-B CASTs

The ATPase activity of AAA+ proteins is often involved in regulating the assembly and recycling of multicomponent molecular systems [57]. Although ATP binding is essential for the oligomeric assembly of TnsC in type I-F CASTs, ATP hydrolysis is not strictly required for transposition, as ATPase-deficient TnsC mutants support reduced, yet detectable levels of transposition *in vivo* [38]. Similarly, in the canonical Tn7 transposon, ATP hydrolysis is not strictly necessary for transposition but has been shown to play a role in target immunity to prevent repeated transposon DNA insertion at the same target site [28, 60, 63, 64]. Our *in vitro* assays reveal that type I-B TnsC does not display detectable ATPase activity in isolation. Moreover, TnsAB does not stimulate the ATPase activity of heptameric TnsC assembled on dsDNA *in vitro* (Fig. 4C and Supplementary Fig. S12), which is consistent with the lack of TnsAB-induced TnsC heptamer disassembly. These results are further supported by the recently reported structure of the PmcCAST TnsABCD complex, in which the TnsC subunits within the heptamer remain bound to intact, i.e. unhydrolyzed, ATP molecules. Together, these findings suggest that in type I-B CASTs, TnsC has low intrinsic ATPase activity, which is not stimulated by interaction with TnsAB, implying that it is required neither for transposase recruitment nor for transposase-catalyzed DNA insertion. This contrasts with the mechanism of type V CAST systems, supported by recent structures of the transpososome holocomplex, in which TnsB recruitment results in ATPase-dependent disassembly of target-nucleated TnsC filaments, to leave 12–16 copies of ATP-bound TnsC bound to the target DNA [32, 33].

ATP hydrolysis by TnsC however does appear to be required for efficient on-target transposition activity of type I-B PmcCAST *in vivo*, as indicated by the loss of detectable transposon insertion upon mutation of the Walker B-motif catalytic glutamate residue. This hints that TnsC might exert ATPase activity at a later step in the transposition process. It is conceivable that ATP hydrolysis is required for transpososome disassembly after donor integration has occurred to facilitate the resolution of the resulting DNA structure by replication-mediated repair of target site duplication gaps. Moreover, the ATPase activity of TnsC might be required to promote the recycling of target binding proteins. The ATPase activity of Tn7 TnsC, and its stimulation by TnsB, has been proposed to mediate target immunity by facilitating TnsC dissociation from the target DNA [60, 64]. This mechanism appears to be contradicted by the apparent stability of the type I-B CAST TnsABCD transpososome holocomplex captured by cryo-EM studies, although it cannot be presently excluded that this state represents a transient intermediate prior to ATPase activation. In the Tn7 system, TnsA inhibits TnsB-induced disassembly [60]. It is conceivable that the observed lack of TnsC disassembly in PmcCAST is due to TnsB being constitutively fused to TnsA, thus offering a plausible explanation to reconcile the mechanistic differences between type I-B CASTs and Tn7. Finally, even though type I CAST systems have been assumed to possess target immunity, recent studies have shown that type I-F systems are capable of inserting multiple copies of donor DNA in the same target locus [66]. The functional role of the TnsC ATPase in type I CAST systems and its coupling to target immunity will thus require further investigation.

Acknowledgements

We thank the University of Zurich Center for Microscopy and Image Analysis for their support with cryo-EM data collection, and S. Kreutzer and the ETH Genome Engineering and Measurement Lab for their help with ddPCR experiments. We would like to thank Seraina Oberli for her help with protein purification and providing type V CAST proteins for analysis.

Author contributions: M.J. conceived the study. M.J., I.Q., and G.F. developed the experimental design. G.F. and K.J.S. carried out protein purification and pull-down experiments. G.F. performed size-exclusion chromatography and negative-stain EM analyses. G.F. and I.Q. prepared cryo-EM samples and collected for the PmcTnsC–dsDNA–AMPPNP complex. G.F. prepared cryo-EM samples and collected cryo-EM data of PmcTnsC–dsDNA–AMPPNP–PmcTnsAB^{hook} complex. G.F. processed cryo-EM data and built atomic models. G.F. and C.C. prepared samples for and performed ddPCR experiments. G.F. performed the ATPase activity assays. M.J., G.F., and I.Q. analyzed the data and wrote the manuscript with input from C.C. and K.J.S.

Supplementary data

Supplementary data is available at NAR online.

Conflict of interest

M.J. is a co-founder, equity holder, and member of the Scientific Advisory Board of Caribou Biosciences, Inc. M.J. is a named inventor on patents and patent applications related to CRISPR genome editing technologies. The other authors have no conflicts of interest to declare.

Funding

This work was supported by the European Research Council (ERC) Consolidator Grant CRISPR2.0 (Grant no. ERC-CoG-820152) and an International Research Scholar award to M.J. from the Howard Hughes Medical Institute. G.F. is part of the Biomolecular Structure and Mechanism PhD Program of the Life Science Zurich Graduate School. I.Q. was supported by EMBO (ALTF 296-2020) and UZH Postdoc Grant postdoctoral fellowships. I.Q. is a Vallee Scholar of the Vallee Foundation and a Society in Science Fellow of the Branco Weiss Foundation, administered by the ETH Zurich. Funding to pay the Open Access publication charges for this article was provided by the University of Zurich.

Data availability

Cryo-EM maps have been deposited in the Electron Microscopy Data Bank under accession codes EMD-50932 (PmcTnsC–dsDNA–AMPPNP), EMD-51458 (PmcTnsC–dsDNA–AMPPNP–PmcTnsAB^{hook}), EMD-50933 (PmcTnsC–dsDNA–AMPPNP, stretched heptameric conformation), and EMD-50934 (PmcTnsC–dsDNA–AMPPNP, stretched octameric conformation). Structural models have been deposited in the Protein Data Bank with accession codes 9G0F (PmcTnsC–dsDNA–AMPPNP) and 9GMZ (PmcTnsC–dsDNA–AMPPNP—PmcTnsAB^{hook}). Source images for negative-stain electron micrographs and gels are included in Supplementary Fig. S15.

References

1. Munoz-Lopez M, Garcia-Perez JL. DNA transposons: nature and applications in genomics. *CG* 2010;**11**:115–28. https://doi.org/10.2174/138920210790886871
2. Hickman AB, Dyda F. DNA transposition at work. *Chem Rev* 2016;**116**:12758–84. https://doi.org/10.1021/acs.chemrev.6b00003
3. Harshey RM, Bukhari AI. A mechanism of DNA transposition. *Proc Natl Acad Sci USA* 1981;**78**:1090–4. https://doi.org/10.1073/pnas.78.2.1090
4. Haren L, Ton-Hoang B, Chandler M. Integrating DNA: transposases and retroviral integrases. *Annu Rev Microbiol* 1999;**53**:245–81. https://doi.org/10.1146/annurev.micro.53.1.245
5. Craig NL. Transposon Tn7. *Curr Top Microbiol Immunol* 1996;**204**:27–48.
6. Peters JE, Craig NL. Tn7: smarter than we thought. *Nat Rev Mol Cell Biol* 2001;**2**:806–14. https://doi.org/10.1038/35099006
7. Peters JE. Targeted transposition with Tn7 elements: safe sites, mobile plasmids, CRISPR/Cas and beyond. *Mol Microbiol* 2019;**112**:1635–44. https://doi.org/10.1111/mmi.14383
8. Waddell CS, Craig NL. Tn7 transposition: recognition of the attTn7 target sequence. *Proc Natl Acad Sci USA* 1989;**86**:3958–62. https://doi.org/10.1073/pnas.86.11.3958
9. Mitra R, McKenzie GJ, Yi L *et al.* Characterization of the TnsD–attTn7 complex that promotes site-specific insertion of Tn7. *Mobile DNA* 2010;**1**:18. https://doi.org/10.1186/1759-8753-1-18
10. Peters JE, Craig NL. Tn7 recognizes transposition target structures associated with DNA replication using the DNA-binding protein TnsE. *Genes Dev* 2001;**15**:737–47. https://doi.org/10.1101/gad.870201
11. Kuduvalli PN, Rao JE, Craig NL. Target DNA structure plays a critical role in Tn7 transposition. *Embo J* 2001;**20**:924–32. https://doi.org/10.1093/emboj/20.4.924
12. Choi KY, Spencer JM, Craig NL. The Tn7 transposition regulator TnsC interacts with the transposase subunit TnsB and target selector TnsD. *Proc Natl Acad Sci USA* 2014;**111**:E2858–65. https://doi.org/10.1073/pnas.1409869111
13. Sarnovsky RJ, May EW, Craig NL. The Tn7 transposase is a heteromeric complex in which DNA breakage and joining activities are distributed between different gene products. *EMBO J* 1996;**15**:6348–61. https://doi.org/10.1002/j.1460-2075.1996.tb01024.x
14. Peters JE, Makarova KS, Shmakov S *et al.* Recruitment of CRISPR–Cas systems by Tn7-like transposons. *Proc Natl Acad Sci USA* 2017;**114**:E7358–66. https://doi.org/10.1073/pnas.1709035114
15. Faure G, Shmakov SA, Yan WX *et al.* CRISPR–Cas in mobile genetic elements: counter-defence and beyond. *Nat Rev Micro* 2019;**17**:513–25. https://doi.org/10.1038/s41579-019-0204-7
16. Strecker J, Ladha A, Gardner Z *et al.* RNA-guided DNA insertion with CRISPR-associated transposases. *Science* 2019;**365**:48–53. https://doi.org/10.1126/science.aax9181
17. Klompe SE, Vo PLH, Halpin-Healy TS *et al.* Transposon-encoded CRISPR–Cas systems direct RNA-guided DNA integration. *Nature* 2019;**571**:219–25. https://doi.org/10.1038/s41586-019-1323-z
18. Petassi MT, Hsieh SC, Peters JE. Guide RNA categorization enables target site choice in Tn7–CRISPR–Cas transposons. *Cell* 2020;**183**:1757–71. https://doi.org/10.1016/j.cell.2020.11.005
19. Saito M, Ladha A, Strecker J *et al.* Dual modes of CRISPR-associated transposon homing. *Cell* 2021;**184**:2441–53. https://doi.org/10.1016/j.cell.2021.03.006
20. Rybarski JR, Hu K, Hill AM *et al.* Metagenomic discovery of CRISPR-associated transposons. *Proc Natl Acad Sci USA* 2021;**118**:e2112279118. https://doi.org/10.1073/pnas.2112279118
21. Hsieh SC, Peters JE. Discovery and characterization of novel type I-D CRISPR-guided transposons identified among diverse Tn7-like elements in cyanobacteria. *Nucleic Acids Res* 2023;**51**:765–82. https://doi.org/10.1093/nar/gkac1216

22. Brouns SJJ, Jore MM, Lundgren M *et al.* Small CRISPR RNAs guide antiviral defense in prokaryotes. *Science* 2008;**321**:960–4. https://doi.org/10.1126/science.1159689
23. Pacesa M, Pelea O, Jinek M. Past, present, and future of CRISPR genome editing technologies. *Cell* 2024;**187**:1076–100. https://doi.org/10.1016/j.cell.2024.01.042
24. Vo PLH, Acree C, Smith ML *et al.* Unbiased profiling of CRISPR RNA-guided transposition products by long-read sequencing. *Mobile DNA* 2021;**12**:13. https://doi.org/10.1186/s13100-021-00242-2
25. Gelsinger DR, Vo PLH, Klompe SE *et al.* Bacterial genome engineering using CRISPR-associated transposases. *Nat Protoc* 2024;**19**:752–90. https://doi.org/10.1038/s41596-023-00927-3
26. George JT, Acree C, Park JU *et al.* Mechanism of target site selection by type V-K CRISPR-associated transposases. *Science* 2023;**382**:eadj8543. https://doi.org/10.1126/science.adj8543
27. Querques I, Schmitz M, Oberli S *et al.* Target site selection and remodelling by type V CRISPR-transposon systems. *Nature* 2021;**599**:497–502. https://doi.org/10.1038/s41586-021-04030-z
28. Park JU, Tsai AW, Mehrotra E *et al.* Structural basis for target site selection in RNA-guided DNA transposition systems. *Science* 2021;**373**:768–74. https://doi.org/10.1126/science.abi8976
29. Schmitz M, Querques I, Oberli S *et al.* Structural basis for the assembly of the type V CRISPR-associated transposon complex. *Cell* 2022;**185**:4999–5010. https://doi.org/10.1016/j.cell.2022.11.009
30. Park JU, Tsai AW, Chen TH *et al.* Mechanistic details of CRISPR-associated transposon recruitment and integration revealed by cryo-EM. *Proc Natl Acad Sci USA* 2022;**119**:e2202590119. https://doi.org/10.1073/pnas.2202590119
31. Tenjo-Castano F, Sofos N, Lopez-Mendez B *et al.* Structure of the TnsB transposase-DNA complex of type V-K CRISPR-associated transposon. *Nat Commun* 2022;**13**:5792. https://doi.org/10.1038/s41467-022-33504-5
32. Park JU, Tsai AW, Rizo AN *et al.* Structures of the holo CRISPR RNA-guided transposon integration complex. *Nature* 2023;**613**:775–82. https://doi.org/10.1038/s41586-022-05573-5
33. Tenjo-Castano F, Sofos N, Stutzke LS *et al.* Conformational landscape of the type V-K CRISPR-associated transposon integration assembly. *Mol Cell* 2024;**84**:2353–67. https://doi.org/10.1016/j.molcel.2024.05.005
34. Halpin-Healy TS, Klompe SE, Sternberg SH *et al.* Structural basis of DNA targeting by a transposon-encoded CRISPR–Cas system. *Nature* 2020;**577**:271–4. https://doi.org/10.1038/s41586-019-1849-0
35. Jia N, Xie W, de la Cruz MJ *et al.* Structure-function insights into the initial step of DNA integration by a CRISPR–Cas–transposon complex. *Cell Res* 2020;**30**:182–4. https://doi.org/10.1038/s41422-019-0272-2
36. Li Z, Zhang H, Xiao R *et al.* Cryo-EM structure of a type I-F CRISPR RNA guided surveillance complex bound to transposition protein TniQ. *Cell Res* 2020;**30**:179–81. https://doi.org/10.1038/s41422-019-0268-y
37. Wang S, Gabel C, Siddique R *et al.* Molecular mechanism for Tn7-like transposon recruitment by a type I-B CRISPR effector. *Cell* 2023;**186**:4204–15. https://doi.org/10.1016/j.cell.2023.07.010
38. Hoffmann FT, Kim M, Beh LY *et al.* Selective TnsC recruitment enhances the fidelity of RNA-guided transposition. *Nature* 2022;**609**:384–93. https://doi.org/10.1038/s41586-022-05059-4
39. Aslanidis C, de Jong PJ. Ligation-independent cloning of PCR products (LIC-PCR). *Nucl Acids Res* 1990;**18**:6069–74. https://doi.org/10.1093/nar/18.20.6069
40. Gibson DG, Young L, Chuang RY *et al.* Enzymatic assembly of DNA molecules up to several hundred kilobases. *Nat Methods* 2009;**6**:343–5. https://doi.org/10.1038/nmeth.1318
41. Punjani A, Rubinstein JL, Fleet DJ *et al.* cryoSPARC: algorithms for rapid unsupervised cryo-EM structure determination. *Nat Methods* 2017;**14**:290–6. https://doi.org/10.1038/nmeth.4169
42. Mirdita M, Schutze K, Moriwaki Y *et al.* ColabFold: making protein folding accessible to all. *Nat Methods* 2022;**19**:679–82. https://doi.org/10.1038/s41592-022-01488-1
43. Jumper J, Evans R, Pritzel A *et al.* Highly accurate protein structure prediction with AlphaFold. *Nature* 2021;**596**:583–9. https://doi.org/10.1038/s41586-021-03819-2
44. Pettersen EF, Goddard TD, Huang CC *et al.* UCSF ChimeraX: structure visualization for researchers, educators, and developers. *Protein Sci* 2021;**30**:70–82. https://doi.org/10.1002/pro.3943
45. Emsley P, Lohkamp B, Scott WG *et al.* Features and development of Coot. *Acta Crystallogr D Biol Crystallogr* 2010;**66**:486–501. https://doi.org/10.1107/S0907444910007493
46. Adams PD, Afonine PV, Bunkoczi G *et al.* PHENIX: a comprehensive Python-based system for macromolecular structure solution. *Acta Crystallogr D Biol Crystallogr* 2010;**66**:213–21. https://doi.org/10.1107/S0907444909052925
47. Brown A, Long F, Nicholls RA *et al.* Tools for macromolecular model building and refinement into electron cryo-microscopy reconstructions. *Acta Crystallogr D Biol Crystallogr* 2015;**71**:136–53. https://doi.org/10.1107/S1399004714021683
48. Schrödinger LLC, DeLano W. The PyMOL Molecular Graphics System, Version 3.0. 2024.
49. Hunter S, Apweiler R, Attwood TK *et al.* InterPro: the integrative protein signature database. *Nucleic Acids Res* 2009;**37**:D211–5. https://doi.org/10.1093/nar/gkn785
50. Soding J, Biegert A, Lupas AN. The HHpred interactive server for protein homology detection and structure prediction. *Nucleic Acids Res* 2005;**33**:W244–8. https://doi.org/10.1093/nar/gki408
51. Miller JM, Enemark EJ. Fundamental characteristics of AAA+ protein family structure and function. *Archaea* 2016;**2016**:9294307. https://doi.org/10.1155/2016/9294307
52. Iyer LM, Leipe DD, Koonin EV *et al.* Evolutionary history and higher order classification of AAA+ ATPases. *J Struct Biol* 2004;**146**:11–31. https://doi.org/10.1016/j.jsb.2003.10.010
53. Walker JE, Saraste M, Runswick MJ *et al.* Distantly related sequences in the alpha- and beta-subunits of ATP synthase, myosin, kinases and other ATP-requiring enzymes and a common nucleotide binding fold. *EMBO J* 1982;**1**:945–51. https://doi.org/10.1002/j.1460-2075.1982.tb01276.x
54. Saraste M, Sibbald PR, Wittinghofer A. The P-loop–a common motif in ATP- and GTP-binding proteins. *Trends Biochem Sci* 1990;**15**:430–4. https://doi.org/10.1016/0968-0004(90)90281-F
55. Puchades C, Sandate CR, Lander GC. The molecular principles governing the activity and functional diversity of AAA+ proteins. *Nat Rev Mol Cell Biol* 2020;**21**:43–58. https://doi.org/10.1038/s41580-019-0183-6
56. Hanson PI, Whiteheart SW. AAA+ proteins: have engine, will work. *Nat Rev Mol Cell Biol* 2005;**6**:519–29. https://doi.org/10.1038/nrm1684
57. Zhang XD, Wigley DB. The 'glutamate switch' provides a link between ATPase activity and ligand binding in AAA plus proteins. *Nat Struct Mol Biol* 2008;**15**:1223–7. https://doi.org/10.1038/nsmb.1501
58. Wendler P, Ciniawsky S, Kock M *et al.* Structure and function of the AAA plus nucleotide binding pocket. *BBA-Mol Cell Res* 2012;**1823**:2–14.
59. Jones DT, Cozzetto D. DISOPRED3: precise disordered region predictions with annotated protein-binding activity. *Bioinformatics* 2015;**31**:857–63. https://doi.org/10.1093/bioinformatics/btu744
60. Skelding Z, Queen-Baker J, Craig NL. Alternative interactions between the Tn7 transposase and the Tn7 target DNA binding protein regulate target immunity and transposition. *EMBO J* 2003;**22**:5904–17. https://doi.org/10.1093/emboj/cdg551
61. Skelding Z, Sarnovsky R, Craig NL. Formation of a nucleoprotein complex containing Tn7 and its target DNA regulates

transposition initiation. *Embo J* 2002;**21**:3494–504. https://doi.org/10.1093/emboj/cdf347
62. Wang S, Siddique R, Hall MC *et al.* Structure of TnsABCD transpososome reveals mechanisms of targeted DNA transposition. *Cell* 2024;**187**:6865–81. https://doi.org/10.1016/j.cell.2024.09.023
63. Bainton RJ, Kubo KM, Feng JN *et al.* Tn7 transposition: target DNA recognition is mediated by multiple Tn7-encoded proteins in a purified *in vitro* system. *Cell* 1993;**72**:931–43. https://doi.org/10.1016/0092-8674(93)90581-A
64. Stellwagen AE, Craig NL. Avoiding self: two Tn7-encoded proteins mediate target immunity in Tn7 transposition. *Embo J* 1997;**16**:6823–34. https://doi.org/10.1093/emboj/16.22.6823
65. Shen Y, Krishnan SS, Petassi MT *et al.* Assembly of the Tn7 targeting complex by a regulated stepwise process. *Mol Cell* 2024;**84**:2368–81. https://doi.org/10.1016/j.molcel.2024.05.012
66. Yang JJ, Yang JW, Zhang YW *et al.* CRISPR-associated transposase system can insert multiple copies of donor DNA into the same target locus. *Crispr J* 2021;**4**:789–98.

Received: September 23, 2024. **Revised:** February 11, 2025. **Editorial Decision:** February 12, 2025. **Accepted:** February 20, 2025